LETTER

Infrared tubular microcavity based on rolled-up GeSn/Ge nanomembranes

To cite this article: Xiang Wu *et al* 2018 *Nanotechnology* **29** 42LT02

IOP Publishing Letters
Nanotechnology
Nanotechnology 29 (2018) 42LT02 (9pp) https://doi.org/10.1088/1361-6528/aad66e

Letter

Infrared tubular microcavity based on rolled-up GeSn/Ge nanomembranes

Xiang Wu[1], Ziao Tian[1], Hui Cong[2], Yang Wang[1], Riyanto Edy[1], Gaoshan Huang[1], Zengfeng Di[3], Chunlai Xue[4] and Yongfeng Mei[1]

[1] Department of Materials Science, State Key Laboratory of ASIC and Systems, Fudan University, Shanghai 200433, People's Republic of China
[2] College of Materials Science and Optoelectronic Technology, University of the Chinese Academy of Sciences, Beijing 100049, People's Republic of China
[3] Shanghai Institute of Microsystem and Information Technology, Chinese Academy of Sciences, Shanghai 200050, People's Republic of China
[4] State Key Laboratory on Integrated Optoelectronics, Institute of Semiconductors, Chinese Academy of Sciences, Beijing 100083, People's Republic of China

E-mail: yfm@fudan.edu.cn

Received 8 June 2018, revised 11 July 2018
Accepted for publication 27 July 2018
Published 14 August 2018

Abstract

Germanium-Tin (GeSn) alloys have attracted great amounts of attention as these group IV semiconductors present direct band-gap behavior with high Sn content and are compatible with current complementary metal oxide semiconductor technology. In this work, three dimensional tubular GeSn/Ge micro-resonators with a diameter of around 7.3 μm were demonstrated by rolling up GeSn nanomembranes (NM) grown on a Ge-on-insulator wafer via molecular beam epitaxy. The microstructural properties of the resonators were carefully investigated and the strain distributions of the rolled-up GeSn/Ge microcavities along the radial direction were studied by utilizing micro-Raman spectroscopy with different excitation laser wavelengths. The values of the strains calculated from Raman shifts agree well with the theoretical prediction. Coupled with fiber tapers, as-fabricated devices present a high quality factor of up to 800 in the transmission spectral measurements. The micro-resonators fabricated via rolled-up nanotechnology and GeSn/Ge NMs in this work may have great potential in photonic micro- and nanodevices.

Keywords: GeSn nanomembranes, rolled-up nanotechnology, micro-resonators, optical microcavity

(Some figures may appear in colour only in the online journal)

1. Introduction

Germanium-Tin (GeSn) is an interesting group IV semiconductor which exhibits direct band-gap behavior with high Sn content [1, 2], leading to great potential applications in photonics [3, 4] and microelectronics [5]. The demonstration of the first GeSn lasing behavior with a Fabry–Perot waveguide cavity structure in 2015 [3], though achieved at low temperatures (below 90 K), put forward the promising prospect of efficient laser sources monolithically integrated on a Si photonic platform [4]. Additionally, the wavelength of light emitted from GeSn lasers lies around 2.3 μm, making it a promising candidate for gas sensing applications [4].

Optical microcavities [6], or micro-resonators, are ubiquitous in modern photonic and optical devices and have attracted considerable research attentions [7, 8]. Such optical structures provide light confinement in a small volume with resonant circulation, and according to different confinement

methods, they can be classified as Fabry–Perot microcavities, whispering gallery mode (WGM) microcavities, distributed feedback microcavities and photonic crystal microcavities [6, 9]. Among all the four categories, WGM microcavities, which confine light with total internal reflections, enjoy the advantages of high quality factor, low mode volume, high sensitivity and the compatibility with various materials [6, 7, 9]. Thus, there have been a broad range of applications based on WGM resonators such as microlasers [10], biochemical sensors [11] and temperature sensors [12]. Additionally, researchers recently showed that the limitation of coupling bandwidth due to conservation of momentum in WGM resonators can be broken by a slightly deformed microtoroid structure, further broadening its applications in nanophotonic circuits and devices [13].

Nevertheless, three dimensional GeSn WGM microcavities with tubular geometries realized by rolling up GeSn nanomembranes (NMs) are rarely involved. On the one hand, WGM microcavities with tubular geometries benefit from the capability of on-chip integration [14] and the uniaxial tensile strain is introduced during the rolling-up process [15, 16]. On the other, rolled-up nanotechnology [17] exhibits innovative applications in photonics [8, 18–21], electronics [22–24], integrated sensing [25], energy storage [26], biology [27], and micro-robotics [28–31]. Besides, rolled-up nanotechnology also enjoys various advantages [7], such as the convenience to optimize performances of devices via rolling NMs with predefined geometry. For example, the resonant modes of a microtubular bottle resonator fabricated by rolling up strained semiconductor bilayers can be tuned by the winding number and the geometry of the lobe [32, 33]. Therefore, the investigations of three dimensional tubular WGM devices based on rolled-up GeSn NMs are of great interests.

In this work, tubular microcavities based on GeSn NMs were fabricated. Following the description of the design and fabrication process, the microstructural characterizations were performed, which presented the information about crystal quality, lattice constant, and element distributions of GeSn. The characterization of the rolled-up GeSn/Ge microcavities via micro-Raman scattering spectroscopy with different excitation laser powers and wavelengths revealed the strain distributions along the radial direction, which agree well with the theoretical prediction. The optical properties of the GeSn/Ge microcavities were also investigated through transmission spectral measurements, exhibiting a Q-factor up to 800 at the wavelength of 1518 nm.

2. Experimental methods

2.1. Growth and characterization of GeSn NMs

In this work, the GeSn NMs were grown on the Ge-on-insulator wafer (GOI wafer, with 30 nm Ge top layer) via molecular beam epitaxy with a nominal thickness of 30 nm. Before the deposition of GeSn NMs, the GOI wafer was rinsed in 9% hydrofluoric acid (HF) solution for 2 min to remove the native oxide layer, and then cleaned in deionized water. During the growth, the substrate temperature was set at 200 °C [34, 35], and the chamber background pressure was set at 2.2×10^{-6} Pa. Thermal processing above 350 °C should be avoided in order to prevent the segregation of Sn [36]. The as-grown GeSn NMs were then cleaned by ultrasonication in actone, ethanol and deionized water for 5 min. After the cleaning, the surface structures of the GeSn NMs were characterized by atomic force microscopy (AFM).

2.2. Fabrication of GeSn/Ge microcavities

As the rolling-up process is compatible with the conventional photolithography processing, the GeSn microcavities in this work were constructed utilizing pre-defined patterns [37]. In detail, a layer of photoresist was spin-coated on the cleaned GeSn NMs at a speed of 3000 r min^{-1}. The plate making machine (Heidelberg, uPG501) was then utilized to create an U-shape pattern on the GeSn NMs [32]. The patterned GeSn NMs were etched using reactive ion etching with a SF_6/C_4F_8 etching gas [3], and then rinsed in ethanol to remove the photoresist.

After the patterning of GeSn NMs, the sample was immersed into a 40% HF solution to selectively remove the sacrificial layer (SiO_2 in GOI wafer). The etching rate is around 60 nm min^{-1} [37]. During the etching process, the top GeSn/Ge bilayer would release and detach from the substrate. Due to the intrinsic strain in the bilayer introduced during the deposition, the released NMs would self-roll-up into tubular microcavities.

2.3. Characterization of GeSn/Ge microcavities

The morphological properties of the as-fabricated microcavities were characterized via scanning electron microscopy (SEM, JEOL JSM-6701F). Transmission electron microscopy (TEM, FEI TECNAI G2 S-TWIN F20) was also utilized to characterized the microstructural properties and element distributions of GeSn/Ge microcavities. Before the characterization by TEM, the sample preparation was conducted via focused ion beam (FIB, FEI Helios NanoLab 600). The thickness of the prepared GeSn/Ge microcavities cross-section was less than 10 nm to meet the requirement for high resolution TEM (HRTEM).

Additionally, the micro-Raman scattering spectroscopy (Horiba JY HR-800) with the 514 nm Ar + laser and 325 nm He–Cd laser as the excitation source was utilized to analyze the strain distributions in GeSn/Ge microcavities.

Eventually, in order to characterize the optical properties of the rolled-up GeSn/Ge microcavities, transmission spectral measurements at near infrared wavelengths (from 1510 to 1560 nm) were performed through the evanescent field coupling method [38]. Details of the preparation of the fiber taper have been presented in [39]. The GeSn/Ge microcavities were adhered to capillaries by silver paste in order to avoid direct contacts between the tapered fibers and any other objects on the substrate. The microcavities were then coupled with the fiber tapers with a gap of ~100 nm. At resonant wavelength, light propagating through the waist of the fiber

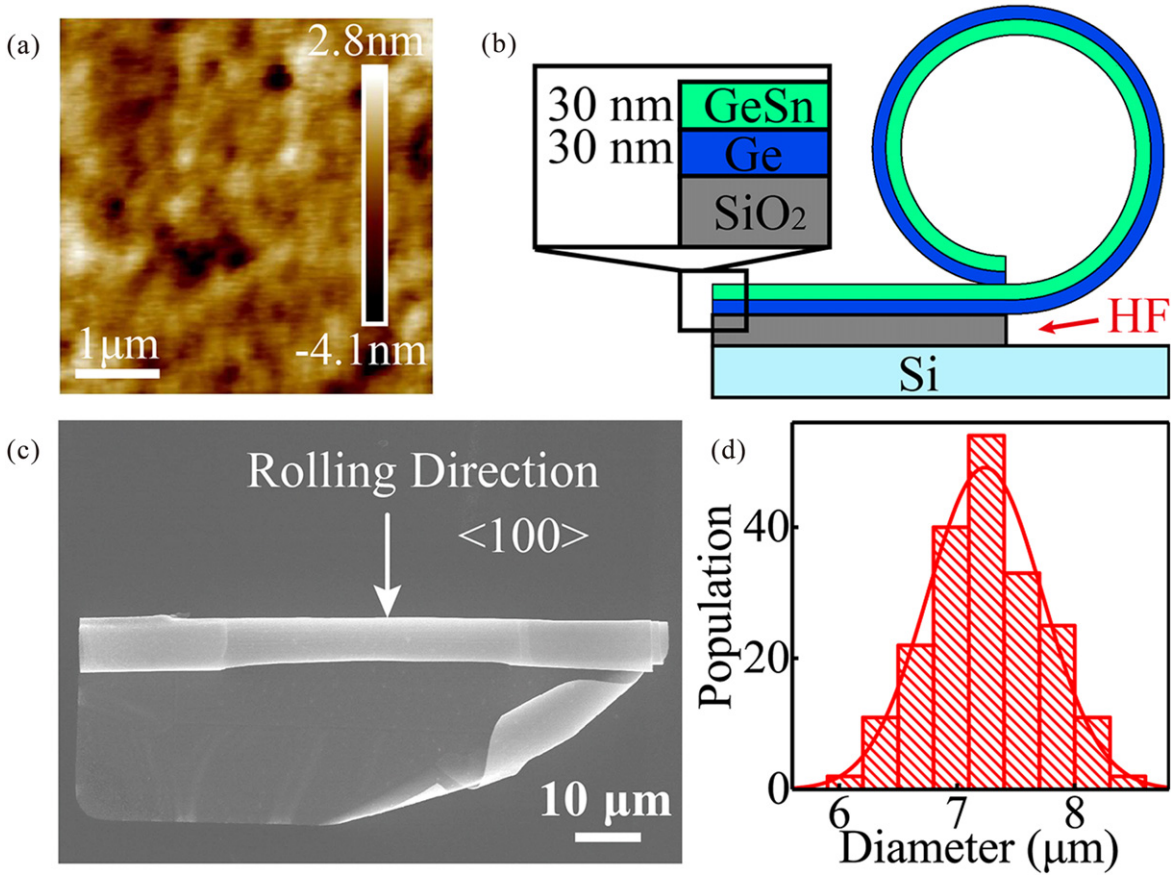

Figure 1. (a) AFM image of GeSn NMs. (b) Schematic diagram illustrating the rolling up process of GeSn/Ge bilayer. The magnified diagram shows the structure of GeSn NMs on GOI wafer. The nominal thicknesses of GeSn and Ge are both 30 nm. (c) SEM image of a typical GeSn/Ge tubular microcavity. The rolling direction (⟨100⟩) of NMs is indicated by a white arrow. (d) Statistics of the diameters of GeSn/Ge microcavities.

taper (with a diameter of approximately 1 μm) tended to escape and enter the microcavity via coupling, leading to Lorentzian-shaped dips in the transmission spectrum.

3. Results and discussion

Figure 1(a) shows the AFM image of GeSn NMs, and the surface roughness (Rq) is measured to be ~0.783 nm, indicating a smooth surface of GeSn NMs. The fabrication process of GeSn/Ge microcavities is illustrated in figure 1(b), while the insert diagram presents the details about sample structure. The typical SEM image of a rolled-up GeSn/Ge tubular microcavity is shown in figure 1(c), and the diameter of the microcavity is measured to be 7.3 μm. Additionally, the repeatability of the fabrication process is clearly illustrated in the statistics of the diameters of microcavities (figure 1(d)). The diameters of microcavities can be tuned by the thickness of the bilayer and the intrinsic strain gradient [17, 40].

The details about microstructure of the as-fabricated GeSn/Ge microcavities are shown in figure 2. The tubular structure of the microcavity is clearly illustrated in figure 2(a). According to the magnified image of the microcavity wall (figure 2(b)), the thicknesses of Ge and GeSn layers are measured to be 27 and 33 nm, respectively. The high crystal quality of Ge layer can be clearly observed in its HRTEM image (the insert of figure 2(b)). The dark part in figure 2(b) is crystalline Ge, while the intervening gray part is supposed to be amorphous due to the damage caused by the Ga ion during FIB. The GeSn layer, however, are mainly amorphous (figure 2(c)) with GeSn nanocrystals (GeSn NCs, figure 2(d)) embedded inside. The scales of NCs are measured to be around 25 nm. The size of NCs can be controlled by the thickness of NMs [41], chamber pressure [42] and substrate temperature [42] during deposition, and can be further tuned by rapid annealing [43, 44] after growth. The (220) lattice plane of GeSn NCs is identified in figure 2(d), and the corresponding interplanar spacing is measured to be $d_{(220)} = 0.204$ nm. Given the lattice constant of Ge ($a_{Ge} = 0.5658$ nm) and α-Sn ($a_{Sn} = 0.6493$ nm), the Sn content in GeSn NCs is calculated to be 13.4% according to the Vegard's law [45]:

$$a_{Ge_{1-x}Sn_x} = (1 - x) \times a_{Ge} + x \times a_{Sn}. \quad (1)$$

Additionally, according to literature [46], under the same Sn content, the lattice constants of crystalline GeSn should be larger than the value calculated from Vegard's law. Thus, the Sn content in present GeSn NCs is supposed to be slightly smaller than 13.4%. The element distributions of Ge and Sn along the dashed red (with GeSn NCs) and green (without GeSn NCs) lines in figure 2(b) are investigated, and the

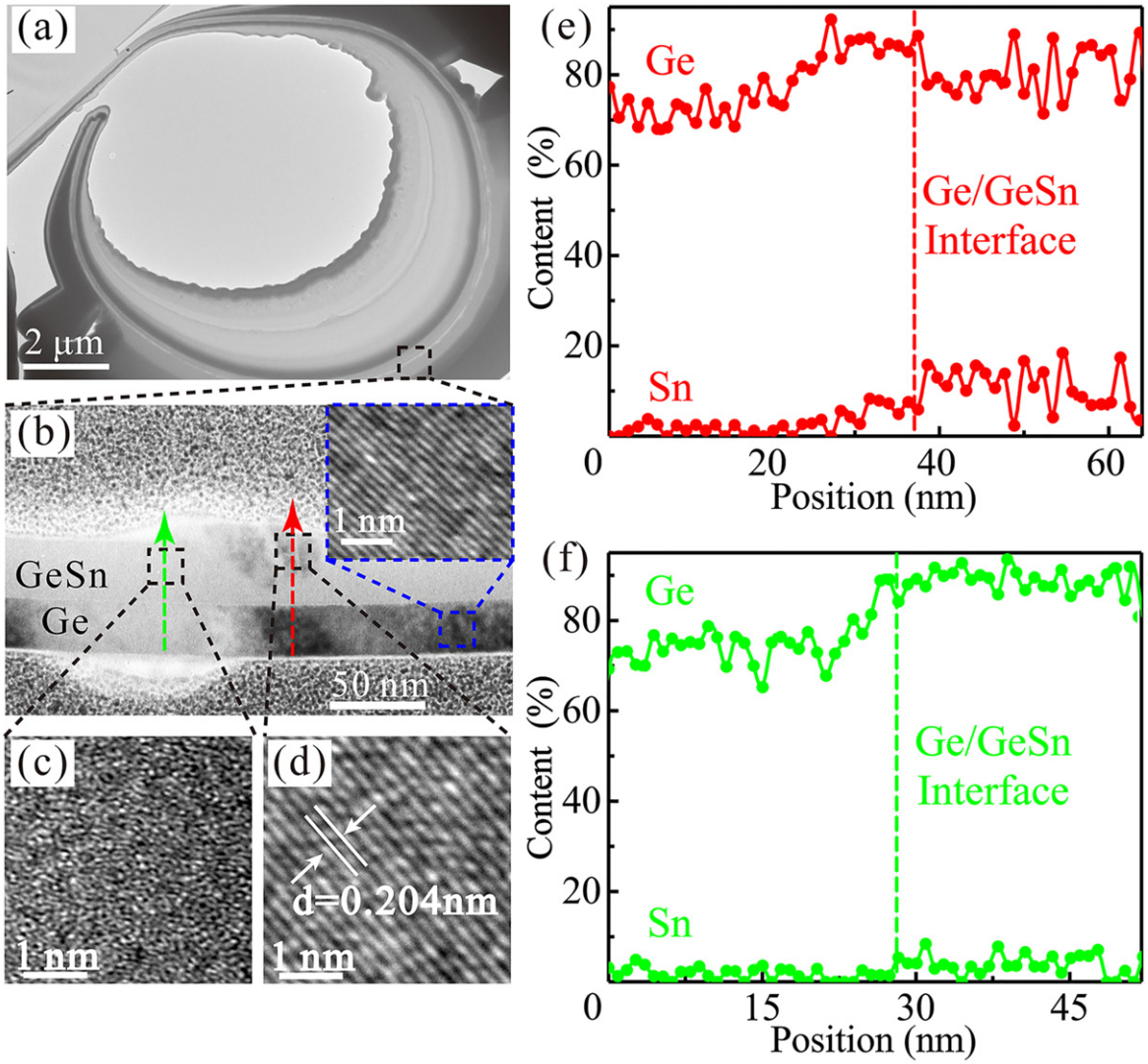

Figure 2. (a) TEM image of the cross-section of a representative GeSn/Ge tubular microcavity. (b) Magnified TEM image of the wall of GeSn/Ge tubular microcavity, showing the bilayer structure of Ge/GeSn. The thicknesses of the Ge and GeSn layers are measured to be 27 and 33 nm, respectively. The insert presents the HRTEM image of the Ge layer, illustrating its high crystal quality. (c) and (d) HRTEM images of the amorphous/crystalline GeSn. The (220) lattice plane in GeSn is indicated with white parallel lines between two opposite arrows, and the corresponding interplanar spacing is highlighted. (e) and (f) Element distributions of Ge and Sn along the dashed red (with GeSn NCs) and green (without GeSn NCs) lines in (b). Ge/GeSn interfaces are marked.

results are presented in figures 2(e) and (f). It is obvious that the Sn content in GeSn NCs is much higher than that in amorphous GeSn (a-GeSn).

Micro-Raman scattering is an effective tool to estimate the strain distributions in semiconductor nanostructures [16, 47]. Figure 3(a) shows a typical Raman spectrum of GeSn NMs excited by the 514 nm laser. The excitation power is set to be 30 mW with a spot size of 1 μm. It should be noted that the Raman spectrum of GeSn NMs can be fitted into two individual sub-peaks. The blue peak centered at 292 cm^{-1} can be attributed to the Ge–Ge mode in GeSn NCs [48], while the green peak centered around 270 cm^{-1} belongs to the Ge–Ge mode in a-GeSn [49], agreeing well with the conclusion drawn from TEM that the GeSn NMs consist of GeSn NCs embedded in a-GeSn. Additionally, according to literature [48, 50], the Sn content in GeSn NCs is estimated to be 12%, which is in accord with the value calculated from Vegard's law.

Furthermore, in order to investigate the strain distributions of the rolled-up tubular microcavities along the radial direction, lasers with two different wavelengths (514 and 325 nm) were applied. It should be noted that the penetration depth of a laser into a certain type of material depends on its wavelength [51]. As schematically illustrated in figure 3(b), the penetration depth of 514 nm laser in Ge is 17.74 nm, while for 325 nm laser the penetration depth is 8.70 nm [15]. Thus, only surface signal can be collected for the 325 nm laser, while signal detected for the 514 nm laser represents an average value in much greater depth. Additionally, when applying micro-Raman scattering to investigate the strain distributions in suspended semiconductor nanostructures (especially tubular microcavities), the local heating

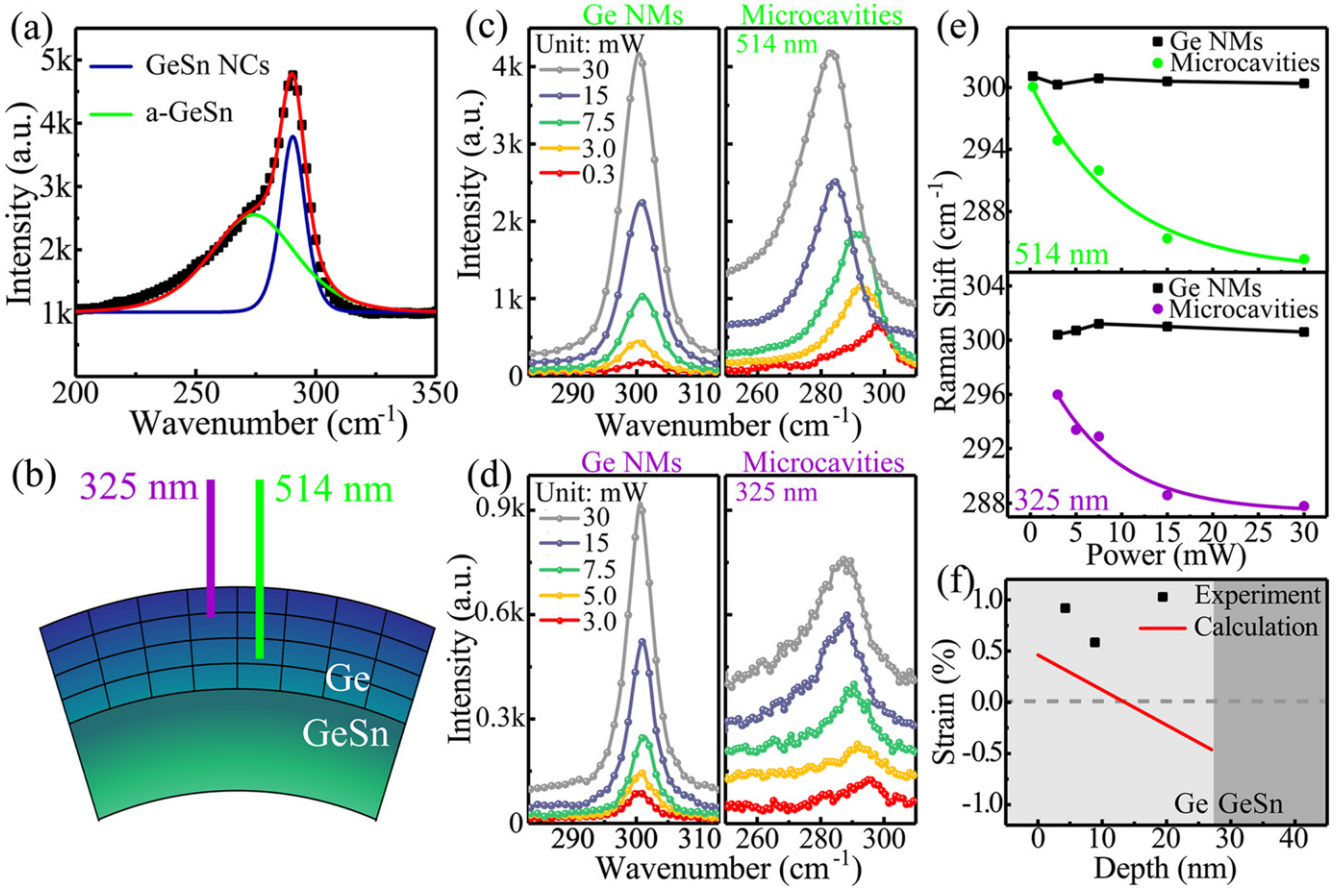

Figure 3. (a) Typical Raman spectrum obtained from GeSn NMs. (b) Schematic diagram showing the different penetration depths of different lasers (i.e., 514 and 325 nm). (c) and (d) Power-dependent Raman spectra collected from Ge NMs (left) and rolled-up GeSn/Ge microcavities (right) excited by lasers with wavelengths of 514 and 325 nm, respectively. (e) The Raman peak positions of Ge–Ge mode in Ge NMs and rolled-up GeSn/Ge microcavities as a function of the excitation power obtained from (c) and (d). (f) Experimental and calculated strain distributions along the radial direction of GeSn/Ge microcavities.

effect should be taken into consideration [16]. Thus, we vary the excitation laser power to eliminate local heating effect and to identify accurately the Raman shifts contributed by the strain.

The power-dependent Raman measurements of Ge NMs (GOI wafer, with a Ge thickness of 25 nm) (left) and GeSn/Ge microcavities (right) excited by 514 and 325 nm lasers are presented in figures 3(c) and (d), respectively. The corresponding Raman peak positions of Ge–Ge mode are summarized in figure 3(e). It is obvious that the Ge–Ge peak positions measured from Ge NMs (marked by black line and points) remain relatively the same despite the variation in excitation power. On the contrary, the Ge–Ge peak positions obtained from GeSn/Ge microcavities excited by both the wavelengths (marked by green and violet dots) shift to lower wavenumber as the excitation laser power increases. Such Raman shift of Ge–Ge peak obtained from GeSn/Ge microcavity should be attributed to the local heating effect, but not due to the different contributions from Ge and GeSn layer, or from GeSn NCs and a-GeSn in GeSn because of the following reasons. Firstly, the Raman signal contributions from different layers and components should not correlate with the excitation power [15, 51]. In other words, the theoretical contributions remain the same despite the variation in laser power. Secondly, the Raman signal contribution from GeSn layer is much smaller than that from Ge layer. Since the laser decays as it propagates through Ge, the laser intensity reaching the Ge/GeSn interface is just 22% of its original value for 514 nm laser, and less than 5% for 325 nm laser. Thus, it is reasonable to assume that the Raman shifts exhibited in figure 3(e) are due to local heating effect.

In order to avoid the local heating effect and to approach the virtual Raman shifts using zero laser power, we apply an exponential fitting and the results are identified by green and violet lines in figure 3(e). By extrapolating the fitted curve into zero laser power, we obtain the virtual Raman shifts. The Ge–Ge peak position obtained from 514 nm laser shifts $\sim -0.89\ \mathrm{cm}^{-1}$ with respect to the bulk Ge peak, and that obtained from 325 nm laser shifts $\sim -1.44\ \mathrm{cm}^{-1}$. Considering phonon deformation potentials [52], the relation between the Raman shifts and the uniaxial strain (ε_{xx}) generated in GeSn/Ge microcavities can be expressed as:

$$\Delta\omega_{\mathrm{bulk}} = -b_{\mathrm{uni}} \times \varepsilon_{xx}, \tag{2}$$

where $\Delta\omega_{\mathrm{bulk}}$ represents the difference of Ge–Ge peak between GeSn/Ge microcavities and bulk Ge, and $b_{\mathrm{uni}} = 154$ is the strain-shift coefficient under purely uniaxial stress situation [53].

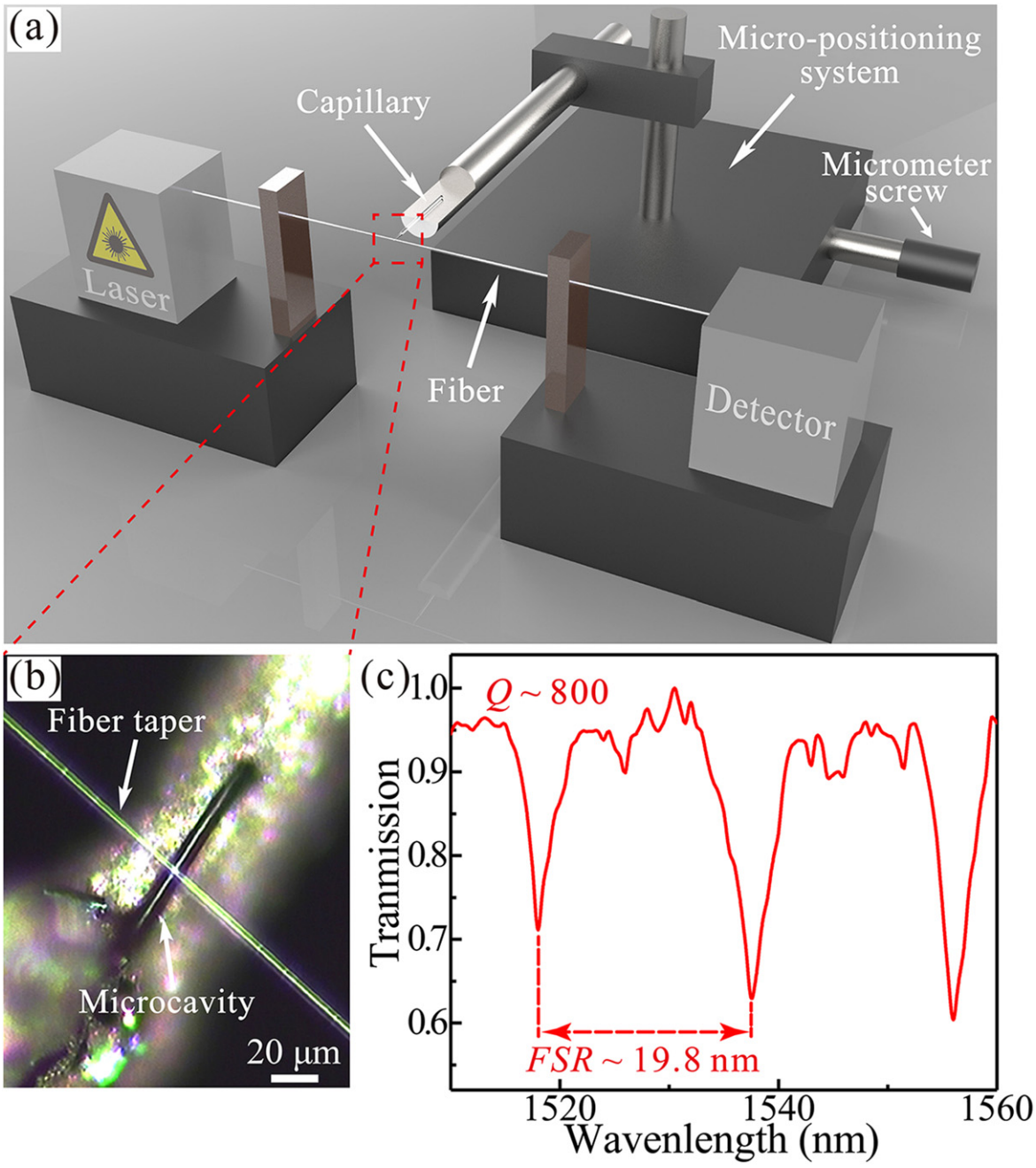

Figure 4. (a) Schematic diagram of the transmission spectral measurements system. The laser, detector, fiber, capillary, micrometer screw and micro-positioning system are marked. (b) Optical microscopy image of a GeSn/Ge tubular microcavity coupled with a vertically placed fiber taper (approximately 1 μm in diameter) for transmission spectral measurements. The microcavity is adhered to a capillary by silver paste. The diameter of the microcavity is measured to be 7.83 μm. (c) A representative transmission spectrum of a tubular GeSn/Ge microcavity, the measured FSR and Q-factor are highlighted.

Therefore, the strain distributions along the radial direction excited by 514 and 325 nm lasers are calculated, and the results are identified by black points in figure 3(f). According to the bending theory [54] and considering the rolling-up process of GeSn/Ge bilayer [16], the outer and inner surfaces of the microcavities are in tension and compression, respectively. Additionally, the theoretical strain distributions along the radial direction can be approximated as linear dependence [15]. In this way, the strain values of rolled-up GeSn/Ge microcavities are calculated and highlighted by the red line in figure 3(f), which are comparable with the values obtained from micro-Raman spectroscopy. The slight discrepancy between the theoretical and experimental results can be attributed to the following reasons. Firstly, focusing the excitation laser spot precisely on the top region of tubular microcavities with small radius is extremely difficult, thus the contribution from sidewall is inevitable [16]. Signals from sidewall are actually detected in a smaller depth than that of signals from the top region, leading to an over-estimation of the tensile strain values. Additionally, the extrapolated Raman shifts may still be different from the virtual

values with zero excitation power, resulting in the perturbation of the obtained strain values.

Eventually, the optical characterization of GeSn/Ge microcavities was carried out via transmission spectral measurements. The schematic diagram of the transmission spectral measurements system is shown in figure 4(a). The vertical position of the GeSn/Ge microcavities could be manipulated by the micro-positioning system with a micrometer screw, and so the gap between the microcavities and fiber could also be controlled. Figure 4(b) shows a microcavity coupled with a fiber taper, and the transmission spectrum of that microcavity is shown in figure 4(c).

The free spectrum range (FSR) is measured to be $\Delta\lambda_{FSR} = 19.8$ nm, which agrees well with the simulation result of $\Delta\lambda_{FSR} = 22.0$ nm using the theoretical formula [39]:

$$\Delta\lambda_{FSR} = \lambda^2/(\pi nD), \quad (3)$$

where the resonant wavelength λ is set as 1537 nm, the refractive index n is set as 4.37 [55], and the diameter of the microcavity D is set as 7.83 μm. The slight discrepancy between the experimental value and the theoretical result can be attributed to the following reasons. Primarily, as there exists a layer of Ge in the rolled-up microcavity, the refractive index of Ge should be taken into consideration. According to [56], the refractive index of a 20 nm thick Ge thin film is measured to be around 4.4 at 1537 nm, and the value is supposed be larger for 30 nm thick Ge. Furthermore, the crystal quality, Sn content and thickness of GeSn is different between this work and [55], leading to the discrepancy in their refractive index. Additionally, the strains inside the GeSn/Ge microcavity would also induce variation of its refractive index. Utilizing Lorenz fitting, the full width at half maximum of the WGM peak centered at 1518 nm is measured to be $\Delta\lambda = \sim 1.91$ nm, corresponding to a Q-factor of 800 according to $Q = \lambda/\Delta\lambda$.

4. Conclusion

In summary, tubular GeSn/Ge micro-resonators were fabricated by rolling up GeSn NMs grown on GOI. Microstructural characterization demonstrated that the GeSn NMs consisted of GeSn NCs embedded in a-GeSn, and the Sn content in GeSn NCs were measured to be slightly less than 13.4%. The strain distributions of the rolled-up GeSn/Ge microcavities were characterized via micro-Raman spectroscopy. The strain obtained from 325 nm laser exhibits larger tensile values than that from 514 nm laser, agreeing well with the bending theory. Transmission spectral measurements through evanescent field method clearly show the resonant behavior of the as-fabricated GeSn/Ge microcavities, which to the best of our knowledge, are the first reported GeSn/Ge micro-resonators based on rolled-up nanotechnology. The Q-factor of GeSn/Ge microcavity reaches as high as 800. Such GeSn micro-resonators based on tubular microcavities could offer a new design route for Si-based integrated light source, and serve as a promising candidate for applications in three dimensional photonic components.

Acknowledgments

This work is supported by the Natural Science Foundation of China (51322201, 61628401, U1632115), Science and Technology Commission of Shanghai Municipality (17JC1401700) and the Changjiang Young Scholars Program of China. X Wu thanks the support from the Fudan Undergraduate Research Opportunities Program (FDUROP, XiYuan 16434 Project). Part of the experimental work was carried out in Fudan Nanofabrication Laboratory.

ORCID iDs

Gaoshan Huang https://orcid.org/0000-0002-0525-7177
Zengfeng Di https://orcid.org/0000-0002-9357-5107
Yongfeng Mei https://orcid.org/0000-0002-3314-6108

References

[1] Mäder K A, Baldereschi A and von Känel H 1989 Band structure and instability of $Ge_{1-x}Sn_x$ alloys *Solid State Commun.* **69** 1123–6
[2] Goodman C H L 1983 Direct-gap group IV semiconductors based on tin *IEE Proc. I Solid State Electron Devices* **130** 46
[3] Wirths S *et al* 2015 Lasing in direct-bandgap GeSn alloy grown on Si *Nat. Photon.* **9** 88–92
[4] Homewood K P and Lourenço M A 2015 Optoelectronics: the rise of the GeSn laser *Nat. Photon.* **9** 78–9
[5] Gupta S *et al* 2016 Density and capture cross-section of interface traps in $GeSnO_2$ and GeO_2 grown on heteroepitaxial GeSn *ACS Appl. Mater. Interfaces* **8** 13181–6
[6] Vahala K J 2003 Optical microcavities *Nature* **424** 839–46
[7] Wang J, Zhan T, Huang G, Chu P K and Mei Y 2014 Optical microcavities with tubular geometry: properties and applications *Laser Photonics Rev.* **8** 521–47
[8] Lin X, Fang Y, Zhu L, Zhang J, Huang G, Wang J and Mei Y 2016 Self-rolling of oxide nanomembranes and resonance coupling in tubular optical microcavity *Adv. Opt. Mater.* **4** 936–42
[9] Yang S, Wang Y and Sun H D 2015 Advances and prospects for whispering gallery mode microcavities *Adv. Opt. Mater.* **3** 1136–62
[10] Pöllinger M, O'Shea D, Warken F and Rauschenbeutel A 2009 Ultrahigh-Q tunable whispering-gallery-mode microresonator *Phys. Rev. Lett.* **103** 053901
[11] Vollmer F and Arnold S 2008 Whispering-gallery-mode biosensing: label-free detection down to single molecules *Nat. Methods* **5** 591–6
[12] Suter J D, White I M, Zhu H and Fan X 2007 Thermal characterization of liquid core optical ring resonator sensors *Appl. Opt.* **46** 389–96
[13] Jiang X, Shao L, Zhang S X, Yi X, Wiersig J, Wang L, Gong Q, Loncar M, Yang L and Xiao Y F 2017 Chaos-assisted broadband momentum transformation in optical microresonators *Science* **358** 344–7
[14] Harazim S M, Bolaños Quiñones V A, Kiravittaya S, Sanchez S and Schmidt O G 2012 Lab-in-a-tube: on-chip integration of glass optofluidic ring resonators for label-free sensing applications *Lab Chip* **12** 2649–55

[15] Guo Q, Wang G, Chen D, Li G, Huang G, Zhang M, Wang X, Mei Y and Di Z 2017 Exceptional transport property in a rolled-up germanium tube *Appl. Phys. Lett.* **110** 112104

[16] Guo Q *et al* 2015 Uniaxial and tensile strained germanium nanomembranes in rolled-up geometry by polarized Raman scattering spectroscopy *AIP Adv.* **5** 037115

[17] Mei Y, Huang G, Solovev A A, Ureña E B, Mönch I, Ding F, Reindl T, Fu R K Y, Chu P K and Schmidt O G 2008 Versatile approach for integrative and functionalized tubes by strain engineering of nanomembranes on polymers *Adv. Mater.* **20** 4085–90

[18] Wang H, Zhen H, Li S, Jing Y, Huang G, Mei Y and Lu W 2016 Self-rolling and light-trapping in flexible quantum well—embedded nanomembranes for wide-angle infrared photodetectors *Sci. Adv.* **2** e1600027

[19] Smith E J, Liu Z, Mei Y F and Schmidt O G 2009 System investigation of a rolled-up metamaterial optical hyperlens structure *Appl. Phys. Lett.* **95** 2007–10

[20] Yu X, Arbabi E, Goddard L L, Li X and Chen X 2015 Monolithically integrated self-rolled-up microtube-based vertical coupler for three-dimensional photonic integration *Appl. Phys. Lett.* **107** 031102

[21] Kerbst J, Schwaiger S, Rottler A, Koitmäe A, Brll M, Ehlermann J, Stemmann A, Heyn C, Heitmann D and Mendach S 2011 Enhanced transmission in rolled-up hyperlenses utilizing Fabry–Pérot resonances *Appl. Phys. Lett.* **99** 191905

[22] Cavallo F, Songmuang R and Schmidt O G 2008 Fabrication and electrical characterization of Si-based rolled-up microtubes *Appl. Phys. Lett.* **93** 2006–9

[23] Yu X, Huang W, Li M, Comberiate T M, Gong S, Schutt-Aine J E and Li X 2015 Ultra-small, high-frequency, and substrate-immune microtube inductors transformed from 2D to 3D *Sci. Rep.* **5** 9661

[24] Grimm D, Bof Bufon C C, Deneke C, Atkinson P, Thurmer D J, Schäffel F, Gorantla S, Bachmatiuk A and Schmidt O G 2013 Rolled-up nanomembranes as compact 3D architectures for field effect transistors and fluidic sensing applications *Nano Lett.* **13** 213–8

[25] Fang Y, Lin X, Tang S, Xu B, Wang J and Mei Y 2017 Temperature-dependent optical resonance in a thin-walled tubular oxide microcavity *Prog. Nat. Sci. Mater. Int.* **27** 498–502

[26] Yan C, Xi W, Si W, Deng J and Schmidt O G 2013 Highly conductive and strain-released hybrid multilayer Ge/Ti nanomembranes with enhanced lithium-ion-storage capability *Adv. Mater.* **25** 539–44

[27] Huang G, Mei Y, Thurmer D J, Coric E and Schmidt O G 2009 Rolled-up transparent microtubes as two-dimensionally confined culture scaffolds of individual yeast cells *Lab Chip* **9** 263–8

[28] Xu B, Zhang B, Wang L, Huang G and Mei Y 2018 Tubular micro/nanomachines: from the basics to recent advances *Adv. Funct. Mater.* **28** 1705872

[29] Xu B and Mei Y 2017 Tubular micro/nanoengines: boost motility in a tiny world *Sci. Bull.* **62** 525–7

[30] Mei Y, Solovev A A, Sanchez S and Schmidt O G 2011 Rolled-up nanotech on polymers: from basic perception to self-propelled catalytic microengines *Chem. Soc. Rev.* **40** 2109–19

[31] Solovev A A, Xi W, Gracias D H, Harazim S M, Deneke C, Sanchez S and Schmidt O G 2012 Self-propelled nanotools *ACS Nano* **6** 1751–6

[32] Strelow C, Schultz C M, Rehberg H, Sauer M, Welsch H, Stemmann A, Heyn C, Heitmann D and Kipp T 2012 Light confinement and mode splitting in rolled-up semiconductor microtube bottle resonators *Phys. Rev.* B **85** 155329

[33] Strelow C, Schultz C M, Rehberg H, Welsch H, Heyn C, Heitmann D and Kipp T 2007 Three dimensionally confined optical modes in quantum-well microtube ring resonators *Phys. Rev.* B **76** 045303

[34] Zhang D, Xue C, Cheng B, Su S, Liu Z, Zhang X, Zhang G, Li C and Wang Q 2013 High-responsivity GeSn short-wave infrared p-i-n photodetectors *Appl. Phys. Lett.* **102** 141111

[35] Richard D'Costa V, Wang W, Zhou Q, Soon Tok E and Yeo Y C 2014 Above-bandgap optical properties of biaxially strained GeSn alloys grown by molecular beam epitaxy *Appl. Phys. Lett.* **104** 022111

[36] Chen R, Gupta S, Huang Y C, Huo Y, Rudy C W, Sanchez E, Kim Y, Kamins T I, Saraswat K C and Harris J S 2014 Demonstration of a Ge/GeSn/Ge quantum-well microdisk resonator on silicon: enabling high-quality Ge(Sn) materials for micro-and nanophotonics *Nano Lett.* **14** 37–43

[37] Tian Z, Zhang L, Fang Y, Xu B, Tang S, Hu N, An Z, Chen Z and Mei Y 2017 Deterministic self-rolling of ultrathin nanocrystalline diamond nanomembranes for 3D tubular/helical architecture *Adv. Mater.* **29** 1604572

[38] Armani D K, Kippenberg T J, Spillane S M and Vahala K J 2003 Ultra-high-Q toroid microcavity on a chip *Nature* **421** 925–8

[39] Li Y, Fang Y, Wang J, Wang L, Tang S, Jiang C, Zheng L and Mei Y 2016 Integrative optofluidic microcavity with tubular channels and coupled waveguides via two-photon polymerization *Lab Chip* **16** 4406–14

[40] Deneke C, Müller C, Jin-Phillipp N Y and Schmidt O G 2002 Diameter scalability of rolled-up In(Ga)As/GaAs nanotubes *Semicond. Sci. Technol.* **17** 1278–81

[41] Mao L F, Zhu C Y, Zhang L J, Ji A M and Liu X Y 2013 Investigation of crystal size impacts on the tunneling current in germanium nanocrystal metal-oxide-semiconductor transistors *Curr. Nanosci.* **9** 103–6

[42] Babu N S and Khadar M A 2018 Electrical properties of grain size tuned CdSe nanocrystal films for practical applications *Sol. Energy Mater. Sol. Cells* **178** 106–14

[43] Pinto S R C, Rolo A G, Chahboun A, Kashtiban R J, Bangert U and Gomes M J M 2010 Raman study of stress effect on Ge nanocrystals embedded in Al_2O_3 *Thin Solid Films* **518** 5378–81

[44] Shen J K, Wu X L, Tan C, Yuan R K and Bao X M 2002 Correlation of electroluminescence with Ge nanocrystal sizes in Ge-SiO_2 co-sputtered films *Phys. Lett.* A **300** 307–10

[45] Vegard L Z 1921 Die Konstitution der Mischkristalle und die Raumfüllung der Atome *Z. Phys.* **5** 17–26

[46] Bauer M, Taraci J, Tolle J, Chizmeshya A V G, Zollner S, Smith D J, Menendez J, Hu C and Kouvetakis J 2002 Ge-Sn semiconductors for band-gap and lattice engineering *Appl. Phys. Lett.* **81** 2992–4

[47] Biswas S, Doherty J, Saladukha D, Ramasse Q, Majumdar D, Upmanyu M, Singha A, Ochalski T, Morris M A and Holmes J D 2016 Non-equilibrium induction of tin in germanium: towards direct bandgap $Ge_{1-x}Sn_x$ nanowires *Nat. Commun.* **7** 11405

[48] Gassenq A *et al* 2017 Raman spectral shift versus strain and composition in GeSn layers with 6%–15% Sn content *Appl. Phys. Lett.* **110** 112101

[49] Zhang L, Wang Y, Chen N, Lin G, Li C, Huang W, Chen S, Xu J and Wang J 2016 Raman scattering study of amorphous GeSn films and their crystallization on Si substrates *J. Non-Cryst. Solids* **448** 74–8

[50] Perova T S, Kasper E, Oehme M, Cherevkov S and Schulze J 2017 Features of polarized Raman spectra for homogeneous and non-homogeneous compressively strained $Ge_{1-y}Sn_y$ alloys *J. Raman Spectrosc.* **48** 993–1001

[51] Takahashi J I and Makino T 1988 Raman scattering measurement of silicon-on-insulator substrates formed by high-dose oxygen-ion implantation *J. Appl. Phys.* **63** 87–91

[52] Mizoguchi K and Nakashima S I 1989 Determination of crystallographic orientations in silicon films by Raman-

microprobe polarization measurements *J. Appl. Phys.* **65** 2583–90
[53] Süess M J, Geiger R, Minamisawa R A, Schiefler G, Frigerio J, Chrastina D, Isella G, Spolenak R, Faist J and Sigg H 2013 Analysis of enhanced light emission from highly strained germanium microbridges *Nat. Photon.* **7** 466–72
[54] Suo Z, Ma E Y, Gleskova H and Wagner S 1999 Mechanics of rollable and foldable film-on-foil electronics *Appl. Phys. Lett.* **74** 1177–9
[55] Tran H *et al* 2016 Systematic study of $Ge_{1-x}Sn_x$ absorption coefficient and refractive index for the device applications of Si-based optoelectronics *J. Appl. Phys.* **119** 103106
[56] Ciesielski A, Skowronski L, Pacuski W and Szoplik T 2018 Permittivity of Ge, Te and Se thin films in the 200–1500 nm spectral range. Predicting the segregation effects in silver *Mater. Sci. Semicond. Process.* **81** 64–7